CORRELATIONS OF NEAR- AND FAR-FIELD ACOUSTIC DATA IN A HIGH-SPEED JET

Jacques Lewalle **Kerwin R. Low** **Mark N. Glauser** **Zachary P. Berger**
Department of Mechanical and Aerospace Engineering
Syracuse University
Syracuse, New York 13244, USA
jlewalle@syr.edu krlow@syr.edu mglauser@syr.edu zpberger@syr.edu

ABSTRACT

The cross-correlations of near- and far-field pressure in a M=0.6 cold jet are oscillatory, which implies some phase-locking. A simple model and synthetic signals show that the locking may be related to the steep attenuation with distance from the near-field sensors. In the near-field, wavelet-based nonlinear filtering separates fluctuations that are recognizable at x/D = 3 and 6 (`matched') from the others ('residue'). This decomposition yields distinct signatures in the cross-correlations. The corresponding time lags and frequencies in the cross-correlations point to several categories of sources and their locations. The interpretation is consistent with the eddy pairing or breakdown (i.e. loss of identity) as the sources of noise for short lags, but the longer time lags require another explanation.

FACILITY AND DATA SPECIFICATIONS

The experiments (Low et al., 2010) are performed in the large scale anechoic jet facility (Tinney et al., 2004) at Syracuse University (Figure 1). The experimental test-bed consists of a 2 inch, Mach 0.6 jet. In the near-field, two arrangements of 5 Kulite pressure transducers are located in azimuthal planes at x/D = 3 and x/D = 6. Figure 1 shows a top view of the location of all the near-field and far-field measurement points. In the far-field, we use 6 G.R.A.S.-type microphones arranged in a boom array, distributed in 15^o increments from the jet axis. The array is located 75 diameters from the center of the jet exit plane. All near- and far-field pressure sensors are sampled at 40.96*kHz* and low-pass filtered at 20.48*kHz*. We process 220 samples of 8192 points.

The compensated power spectra for the near- and far-field signals are shown on Figure 2. The magnitudes have been reset for graphical convenience. The far-field noise exhibits the relatively-narrow peak closer to the axis, associated with near-field coherent eddies, superposed on the near-isotropic broader-band noise traceable to the random turbulent mixing.

NEAR/FAR-FIELD CROSS-CORRELATIONS

Cross correlations are one measure of how the near-field pressure relates to the far-field sound. We present results for individual near-field sensors and for their Fourier-filtered modes (mode 0 is axisymmetric). Figure 3 shows the cross correlations of all near field sensors at $x/D = 3$ and 6, and each far field microphone. The plot illustrates the increase of the correlation between the near and far field, as the polar angle goes from 90^o *to* 15^o. Also evident, is the difference in the magnitude of the correlation at the two downstream locations; the array at $x/D = 6$ having a higher correlation than the one at *3*. Figure 4 shows that mode 0 (the average of signals for each set of 5 sensors, i.e. axisymmetric) dominates the cross-correlations. The lags diminish with decreasing polar angle, illustrating the directional nature of the jet acoustics.

Local Frequency of Cross-Correlations

The frequency of the oscillations in the cross-correlations is analyzed next. The cross-correlation is a short signal amenable to further processing; zero-padding was used to alleviate end-effects. The 15 and 90^o cases will illustrate the results. The Morlet wavelet transform (Lewalle et al., 2007) is used for this purpose, because its locally-periodic shape provides good frequency resolution. Successively, we calculated the norm of the transform in the time-frequency domain, identified the ridge lines, and plotted, for each lag, the frequency corresponding to the largest ridge-line energy density (the locally-dominant frequency). The result is shown on Fig 5. When ridge-lines are relatively close in frequency, they tend to shift gradually; a larger spectral gap lets them evolve independently, with abrupt jumps reflecting the change in their relative magnitudes when several ridge lines coexist. The shorter lags for the x/D = 3, relative to x/D = 6, are due to the larger sound propagation speed along the jet. The 15^o lags peak in the same range (10 ms) but different frequencies for the two microphones. The x/D=3, 15^o case shows an abrupt switch in dominant frequency corresponding to the primary oscillation; the similar transition for x/D=3, 90^o, is more gradual. No such transitions are also visible for the x/D = 6 correlations. This is evidence of important changes occurring in the jet between the two near-field stations. It is worth noting that enormous differences occur from sample to sample, we will return to this in the Discussion.

Modelling the Oscillatory Cross-Correlations

In order to gain insight in these changes, we need to understand how presumably random near-field sources can yield oscillatory cross-correlations with the far-field. This implies some mechanism for phase-locking, for which we propose the following model.

Imagine a source in the near-field. The sound it produces propagates toward the kulites and toward the microphones, with steep attenuation. For a periodic source, its motion with Mach number M in the direction of propagation results in a Doppler shift. Thus, the near-field pressure would be

$$p_{NF} \approx A e^{2i\pi\left(\frac{\omega}{1+M}t+\phi\right)} \qquad (1)$$

while the far-field pressure is given by

$$p_{FF} \approx a e^{2i\pi\left(\frac{\omega}{1-M}t+\psi\right)} \qquad (2)$$

The phases are arbitrary, while the magnitudes are affected differently by attenuation: as source location varies, A is strongly affected while a is constant at first order. Ignoring the normalization factor, the cross-correlation of these signals,

$$\int p_{NF}^{*}(t+\tau)\,p_{FF}(t)dt = \int A^{*}ae^{2i\pi(\psi-\phi)}e^{-2i\pi\frac{\omega\tau}{1+M}}e^{2i\pi\frac{2M\omega t}{1-M^{2}}}dt \quad (3)$$

vanishes because of the last factor in the integrand. However, if the oscillation of the source is localized in time, e.g. under a Gaussian envelope:

$$p \approx e^{2i\pi\omega t}e^{-\left(\frac{2\pi\omega t}{z_o}\right)} \quad (4)$$

the corresponding time localization of the pressure signals introduces a factor

$$e^{-\left(\frac{\pi\omega\tau}{z_0}\right)^{2}\left(\frac{(t/\tau+1)^{2}}{(1+M)^{2}}+\frac{t^{2}/\tau^{2}}{(1-M)^{2}}\right)} \quad (5)$$

in the integrand, which restricts the effective contributions to the correlation integral to a narrow range of times and lags. The phase difference varies randomly with the location of the source, but the near-field attenuation will favor the sources closest to the kulites, and this accounts for the oscillation of the cross-correlation. The frequency of this oscillation is, within a Doppler shift, typical of the frequency of the source.

This is more easily seen with a synthetic signal. We generated randomly located pulse-like and oscillatory sources, and modelled the propagation and attenuation of each to the respective sensors. They were then added to Gaussian white noise (independent for the near- and far-field) and the cross-correlations were evaluated. The result is shown on Figure 6.

The propagation times *T* from a hypothetical source to the various sensors was calculated as follows. For small M and an isothermal jet, the sound propagation would be along straight lines at the nominal speed of sound. As M increases, the sound will also be convected along with the local air mass, and an effective sound speed *c* is calculated as the sum of the nominal speed and the component of mean jet speed along the line of sight from source to sensor, with incremental distance *ds*; the refraction and subsequent lengthening of the acoustic path is neglected. Thus

$$T = \int_{source}^{sensor} ds/c \quad (6)$$

The expected lags between near- and far-field signals are shown on Figure 7. The results are not very sensitive to variants in the transition from top-hat velocity profile at the nozzle to bell-shaped self-similar profiles far downstream. The general order of magnitude in the 10ms range is encouraging. Comparing Figures 5 and 7, the later rise of correlation levels, around 11 ms lags, is consistent with the corresponding sources being close to x/D=3 (purple) and x/D=6 (cyan) for the 90^{o} correlations, respectively. At 15^{o}, the flatter green curve (x/D=6) makes it difficult to pinpoint the corresponding sources, but the black curve a dominant range for x/D~3 sources at 1kHz, with additional contributions throughout the range of source locations.

From the combination of synthetic signal, actual data and modelling of the acoustic lags, we conclude that the cross-correlations isolate the contributions from the sources located closest to the kulites, with all other contributions lost to phase-scrambling. Furthermore. the dominant frequencies of the oscillations point to dramatic changes in source properties between x/D = 3 and 6.

NEAR/FAR-FIELD DECOMPOSITION

This prompts further analysis of the near-field traces. We limit ourselves to mode 0, having ascertained that mode 1 yields similar but weaker results. The starting idea is to detect changes between the two stations. If we imagine a pressure fluctuation as resulting from a flow structure being convected near the sensor, recognizing its pings on the successive rings of kulites is achieved with wavelet-transformed signals. Looking for individual pings rather than for wave packets, we used the Mexican hat wavelet (Lewalle et al., 2007). The corresponding coefficients are shown on Figure 8, red is for positive coefficients and blue negative; the square of the coefficients is proportional to the energy density per unit time and per octave, so the brighter patches show energetic (loud) events. Interpreting the wavelet transform as a band-pass filter, each line on Figure 8 is a filtered signal with good time resolution and moderate frequency resolution.

Near-Field Event Recognition

When two such plots are compared for x/D=3 and 6, some events match, with a lag related to the convection time between the stations. The convection speed can be obtained from the cross-correlation of the signals; a mean *frequency-dependent* convection speed is similarly obtained by cross-correlating the band-pass filtered signals. The frequency-dependent cross-correlation is shown on Figure 9, where the ridge (darkest reds) pinpoint the optimal lag, inversely proportional to the convection speed. The lag at frequencies larger than 1kHz is 40 time steps and corresponds to a speed of 0.7 V_j, where V_j is the nominal nozzle velocity (M = 0.6); at 200Hz, the convection speed is only half as large. This matches the expectation that larger structures are located at larger radial distances from the axis and are therefore convected at slower speeds.

This provides recognition between the two near-field stations at a statistical level. Event-by-event recognition is achieved as follows. We take the wavelet transforms at the two stations, and select a given frequency. Then, we offset the two traces by the appropriate lag, and take their product at each time. For perfectly matched signals, these products would all be non-negative. We run the product through a Gaussian filter to smooth out the passages to zero, and threshold the result to keep the larger contributions, i.e. the matched loud events. Repeating at each frequency, we produced the mask shown on Figure 10.

The procedure is repeated with the mean convection speed calculated for each sample – reproducible with little scatter at large frequencies, and with some scatter for the rare low-frequency events. The masks are distinct for each pair of signals, and distinct (though very similar) for x/D=3 and 6.

Far-Field Signature of Matched/Residue Events

The mask (Figure 10) is used for non-linear filtering of the signals (Schobeiri et al., 2003): all wavelet coefficients located at times and frequencies where the mask exceeds the threshold are retained, all others are set to zero. The remaining coefficients (i.e. information about recognized events) are inverse-transformed to produce a filtered pressure signal containing mostly recognized (matched) events, while the difference with the original signal contains mostly events that are not recognized (residue). The results presented below are not very sensitive to the threshold; we will return to this issue in the Discussion. An example of matched trace (Figure 11) shows broad-band intermittent activity. The entire near-field database was processed to yield matched signals and residue for further analysis.

The relevance of this decomposition needs to be established. First, we look at the cross-correlation signatures of the matched signals and residue with the far-field. The result is shown on Figure 12. The differences are striking. For the residue x/D=6, 15^o correlation (green trace), the arrival time is just under 10ms, whereas its matched counterpart is not observed in the far-field, on average, until 12.5ms have passed. Their frequencies, however, are comparable, of the order of 600 Hz.

We propose an interpretation of these results based on the hypothesis that the sound-producing event is the breakdown or other disappearance of a flow structure, maybe a vortex ring. Matching (or not) the passage of the structure near the sensors is distinct from recording the noise it produces upon breaking down. We may not identify the breakdown noise at the near-field sensors, we only recognize their statistical footprints in the cross-correlations: the phase-locking isolates the breakdown noise from the random background which includes the passing of structures. For events to be matched at x/D = 3 and 6, the breakdown must have taken place upstream of x/D=3 or downstream of x/D = 6, and it will contribute to the cross-correlation with far-field noise if it is close enough to the corresponding sensor. The corresponding propagation times would the same as were calculated on Figure 7.

The resulting scenarios are consistent with the measurements, with one significant exception: no combination of lags resulting from sound propagation reaches into the 12.5 to 14 ms range measured for the matched signals at x/D=6. This indicates that one part of the scenario still eludes us. The other combinations confirm the scenario of the sound-producing event (source location) corresponding to a loss of eddy identity (residue, if the breakdown occurs between the near-field stations). Assigning source location remains imprecise, with the ranges $3<x/D<6$, larger, and smaller, as the broad categories.

Frequency-Dependent Cross-Correlations

Consistently with the Parseval theorem for wavelets (e.g. Lewalle et al., 2007), the cross-correlations can also be calculated for the band-pass-filtered signals (original, matched or residue). The results (Figures 13 and 14) obtained from Mexican-hat coefficients, and with Morlet coefficients on Figure 15, are consistent with the above as far as frequencies and typical lags for all combinations of near- and far-field locations, matched and residue, are concerned. For large lags (~13ms, say), we confirm that x/D=6-matched exhibits these unexplained lags; furthermore, we see a secondary clump of similar correlations for x/D=6-residue, which, in retrospect, is also visible on Figure 12. It is not clear at this time if this is due to some matched events remaining in the residue because of an imperfect decomposition, or if the same missing scenario for long lags also applies to the residue.

DISCUSSION

In this paper, we have developed a number of new tools that shed some on the connection between jet noise and its near-jet sources.

The modeling of the oscillatory cross-correlations does not show that the near-field sensors only hear the nearest sources, but that these account for the cross-correlations with the far-field; sources farther away from the kulites may be observed in both near- and far-field, but with random phases that yield no correlation.

The other contributions are dependent, in one way or another, on the time-frequency decompositon (wavelet transform) of the signals. The Mexican hat (good time resolution) and Morlet transforms (good frequency resolution) unravel some of the complexity of the data; we were unable to achieve anything similar with orthogonal wavelets – the Daubechies-2 result for inverse convection speed, Figure 16, did not lead to a useful decomposition of near-field signals. The redundancy of the continuous wavelets turns out to be an asset in eliciting information from the data. The extraction of intermitent dominant cross-correlation freqencies, and the transitions over short lag differences, takes advantage of the properties of the Morlet wavelet. In the near-field, the determination of frequency-dependent convection speed is consistent with current knoweldge, and is used to match individual events between the two stations.

Thesholding, for the nonlinear filtering of matched events, is justified primarily by the striking difference in properties of the resulting signals. We ascertained that changes in threshold result in gradual but not dramatic differences in results, and the choice of threshold adopted here reflects a reasonable decision more than a scientifically justified cut-off.

Sample-to-sample variability for the cross-correlations, not shown because of space constraints, is dramatic. Sample contributions to Figures 12-15 show large patches of highly correlated fluctuations, shifting from sample to sample: we do not see at the sample level the shadow of the ensemble average, whereas, say, the shape of the mean power spectrum emerges from the sample-level scatter. This indicates that the ensemble statistics summarize but also conceal contributions from many different types of events, the properties of which are currently being studied.

The attribution of near/far-field correlated events to specific regions of the near jet is dependent on the modeling of sound propagation and the calculation of corresponding lags. It shows promise towards characterizing broad categories of sources in terms of typical frequency, location, and other parameters. The effect of refraction by mean velocity and temperature profiles is currently being implemented, but we expect only small corrections to the straight-line propagation times. So the large lags (12.5-14 ms) measured in the data make us leave on speculative note: what kind of event would leave footprints in the near-field as it is convected by the kulites, but would become a noise source *farther downstream* (hence the increased lag) *while remaining in-phase* with itself? Maybe a wave packet in a shear layer?

ACKNOWLEDGMENTS

The support of AFOSR under grant FA-9550-10-1-0536 (JL, MNG) and of Syracuse University through a Graduate Fellowship (KRL) is much appreciated.

REFERENCES

Hall, J., Pinier, J., Hall, A.M. and Glauser, M.N. ``Cross-Spectral Analysis of the Pressure in a Mach 0.85 Turbulent Jet,.. AIAA Journal, Vol. 47, No. 1, pp 54-59., 2009.

Koenig, M., Cavalieri, A., Jordan, P., Delville, J., Gervais, Y., Papamoschou, D., Samimy, M. and Lele, S., 'Farfield filtering and source imaging for the study of jet noise', Proc. 16th AIAA Aerosacoustics Conference, AIAA paper 2010-3779 1-24, 2010.

Lewalle,J. Farge, M. and Schneider, K., 'Wavelets', *Springer Handbook of Experimental Fluid Mechanics* (Tropea, Yarin and Foss, Editors), Springer, 2007.

Low, K.R., El-Hadidi, B., Andino, M.Y., Berdanier, R. and Glauser, M.N., 'Investigation of different active flow control strategies for high speed jets using synthetic flow actuators', AIAA Paper 2010-4267, 2010.

Schobeiri, M.T., Reid K. and Lewalle, J., 'Effect of unsteady wake passing frequency on boundary layer transition, experimental investigation and wavelet analysis', J. Fluids Eng. Vol. 125, 251-266, 2003.

Tinney, C.E., Hall, A.M., Glauser, M.N. Ukeiley, L.S., Coughlin, T., 'Designing an anechoic chamber for the experimental study of high speed heated jets', AIAA Paper 2004-0010, 2004.

Ukeiley, L., Seiner, J., Ponton, M., 'Azimuthal structure of an axisymetric jet mixing layer', ASME FEDSM99-7252, (1999) July.

Tinney, C. E., Glauser, M. N., and Ukeiley, L. S., 'Low-dimensional characteristics of a transonic jet Part 1. Proper orthogonal decomposition', J. Fluid Mech Vol. 612, pp. 107-141, 2008.

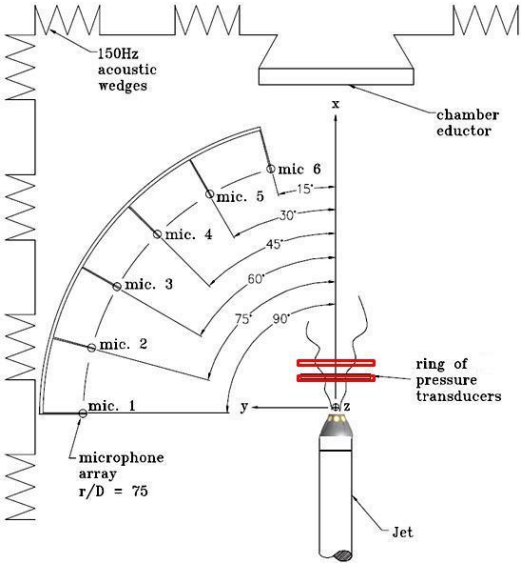

Figure 1: Experimental Setup

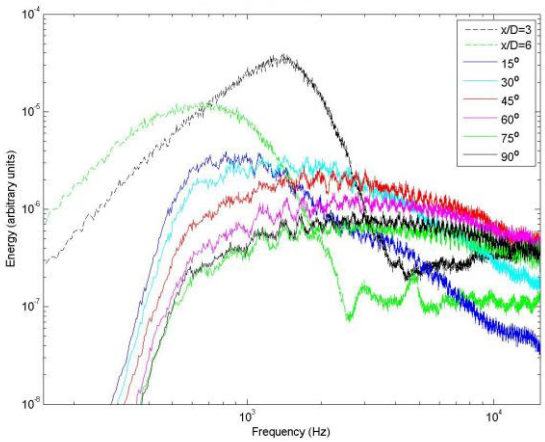

Figure 2: Near- and far-field compensated spectra; near-field energy level is rescaled to fit the plot.

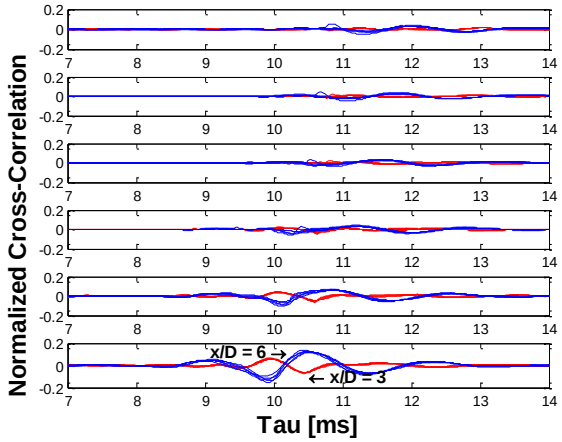

Figure 3: Cross correlation between near field pressure and far field microphones from $\varphi = 90^o$ to $\varphi = 15^o$

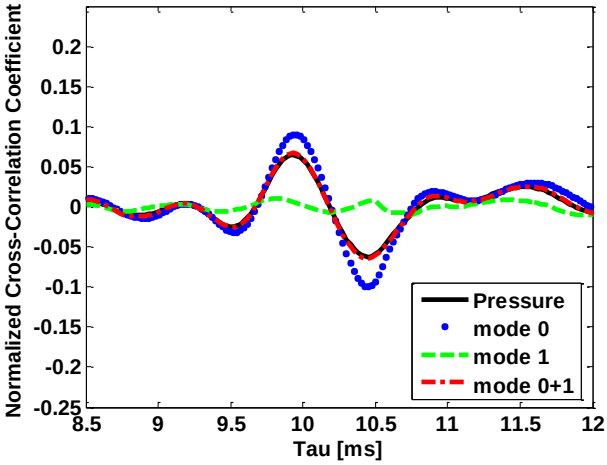

Figure 4: Cross correlation between the mode-filtered near field pressure (x/D = 3) and far field sound at $\varphi = 15^o$.

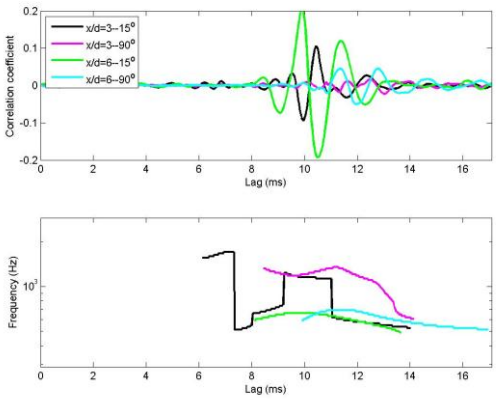

Figure 5: Cross correlation of mode 0 at x/D = 3 and 6 with far field sound at φ = 15 and 90^o (top), and the time-dependent dominant frequency.

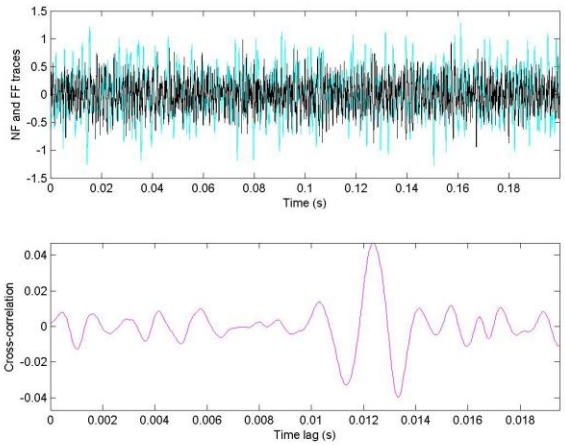

Figure 6: Synthetic signals (top) and their oscillatory cross-correlation (bottom).

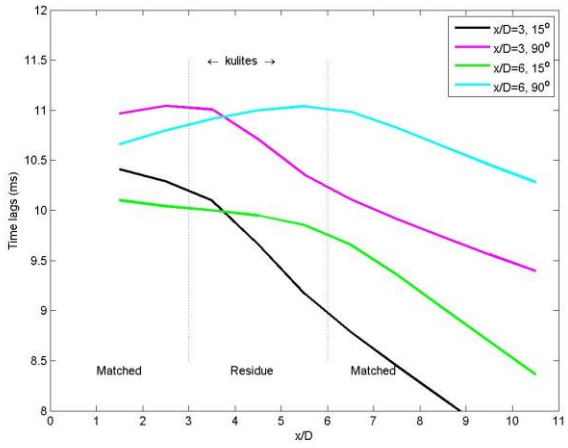

Figure 7: Calculated near/far-field lags as function of axial source location

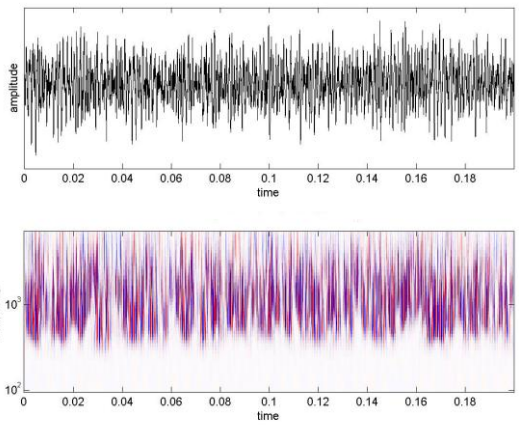

Figure 8: Typical near-field pressure signal and its Mexican hat wavelet coefficients.

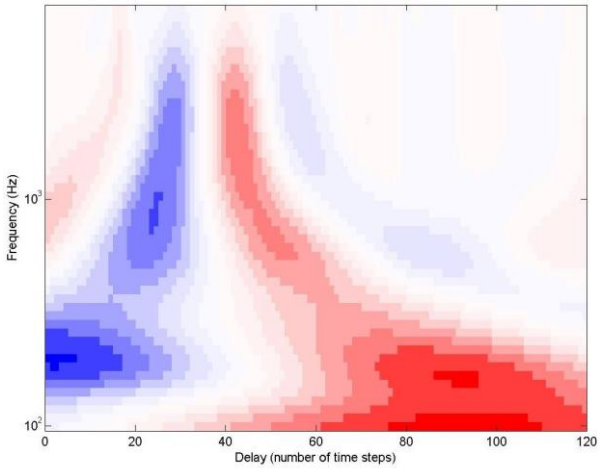

Figure 9: Frequency-dependent cross-correlation between x/D = 3 and 6. Red indicates positive correlations.

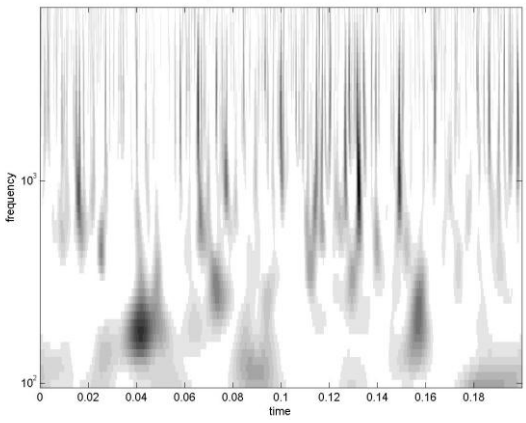

Figure 10: Sample mask of event recognition: dark areas show agreement between the two signals, white areas are not recognizable.

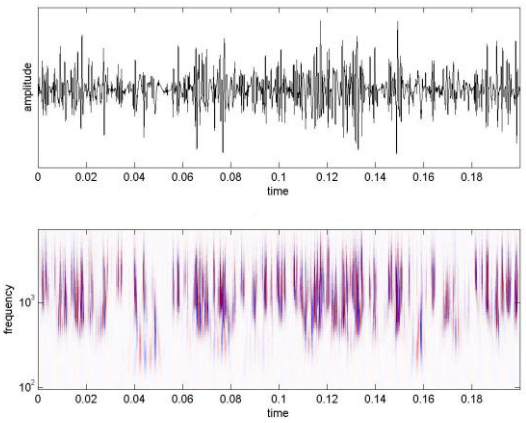

Figure 11: The intermittent matched-event signal and its Mexican hat wavelet coefficients obtained by nonlinear filtering of the Fig. 8 sample.

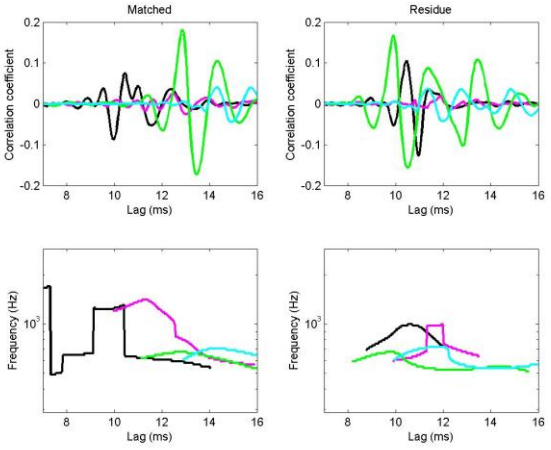

Figure 12: Cross-correlation and dominant frequencies of the matched signals and residue with the far-field (color coding same as for Figs. 5 and 7).

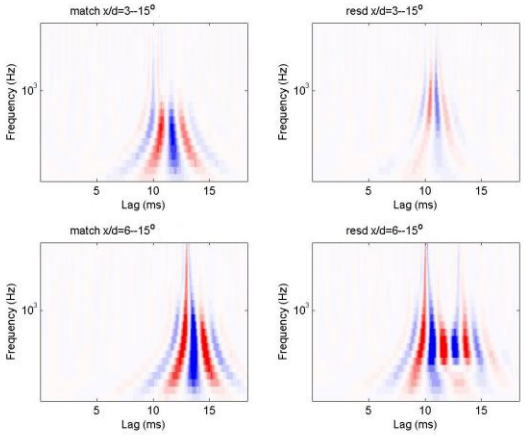

Figure 13: Cross-correlation of Mexican hat coefficients of near-field signals with the far-field at 15°.

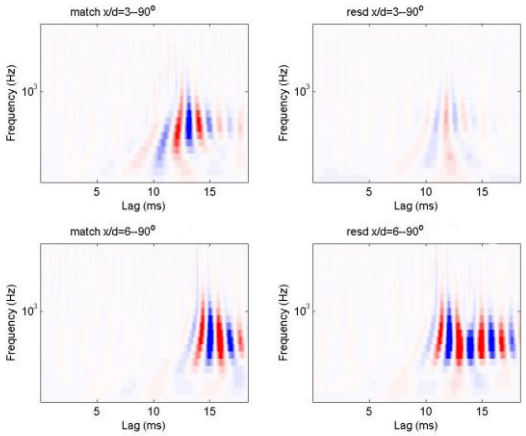

Figure 14: Cross-correlation of Mexican hat coefficients of near-field signals with the far-field at 90°.

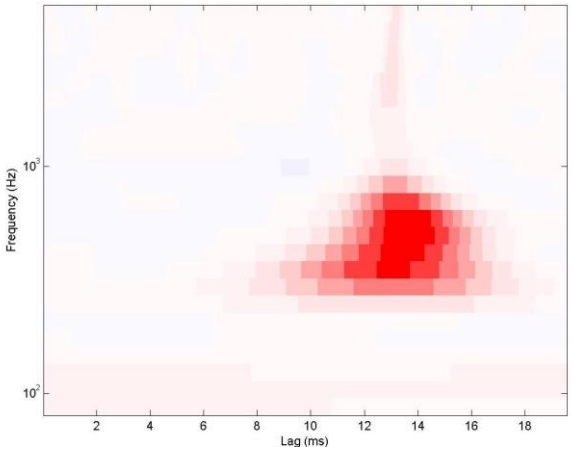

Figure 15: Cross-correlation of Morlet coefficients of near-field matched signals at x/D=6 with the far-field at 15°.

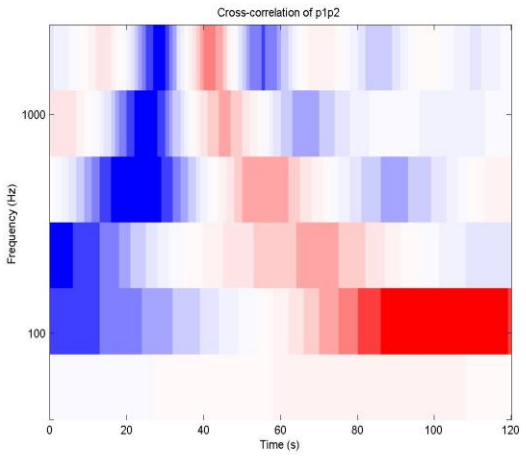

Figure 16: Frequency-dependent cross-correlations with D2 wavelets, similar to Fig. 9; wavelet coefficients are rescaled to be proportional to magnitude per unit time and octave.